MdUGT88F1-Mediated Phloridzin Biosynthesis Regulates Apple Development and *Valsa* Canker Resistance[1][OPEN]

Kun Zhou,[2] Lingyu Hu,[2] Yangtiansu Li, Xiaofeng Chen, Zhijun Zhang, Bingbing Liu, Pengmin Li, Xiaoqing Gong,[3] and Fengwang Ma[3,4]

State Key Laboratory of Crop Stress Biology for Arid Areas/Shaanxi Key Laboratory of Apple, College of Horticulture, Northwest A&F University, Yangling, Shaanxi 712100, China

ORCID IDs: 0000-0003-3514-0153 (P.L.); 0000-0003-3890-2125 (F.M.).

In apple (*Malus domestica*), the polyphenol profile is dominated by phloridzin, but its physiological role remains largely elusive. Here, we used *MdUGT88F1* (a key *UDP-glucose:phloretin 2′-O-glucosyltransferase* gene) transgenic apple lines and *Malus* spp. germplasm to gain more insight into the physiological role of phloridzin in apple. Decreasing phloridzin biosynthesis in apple lines by RNA silencing of *MdUGT88F1* led to a series of severe phenotypic changes that included severe stunting, reduced internode length, spindly leaf shape, increased stem numbers, and weak adventitious roots. These changes were associated directly with reduced lignin levels and disorders in cell wall polysaccharides. Moreover, compact organization of tissues and thickened bark enhanced resistance to *Valsa* canker (caused by the fungus *Valsa mali*), which was associated with lignin- and cell wall polysaccharide-mediated increases of salicylic acid and reactive oxygen species. Phloridzin was also assumed to be utilized directly as a sugar alternative and a toxin accelerator by *V. mali* in apple. Therefore, after infection with *V. mali*, a higher level of phloridzin slightly compromised resistance to *Valsa* canker in *MdUGT88F1*-overexpressing apple lines. Taken together, our results shed light on the importance of MdUGT88F1-mediated biosynthesis of phloridzin in the interplay between plant development and pathogen resistance in apple trees.

Plants are exposed naturally to a large range of biotic and abiotic stresses and, therefore, they need to optimize their fitness by fine-tuning resource allocation for growth and defense (Huot et al., 2014). Plants frequently adopt a comprehensive defense against pathogen/pest threats at the expense of growth (Huot et al., 2014). A large number of structurally diverse molecules involved in plant-pathogen interactions and plant growth are produced by the phenylpropanoid pathway. The phenylpropanoid-derived polymer lignin is produced by oxidative polymerization of three monolignol precursors: *p*-coumaryl alcohol (H unit), coniferyl alcohol (G unit), and sinapyl alcohol (S unit); lignin cross-links plant secondary cell walls to provide mechanical strength and hydrophobicity to the vascular system necessary for the plant's ability to grow upward (Nakashima et al., 2008; Vanholme et al., 2008; Van Acker et al., 2013; Fig. 1). Frequently, interference with lignin biosynthesis leads to growth defects. Intriguingly, lignin-reduced plants exhibit an increase in both salicylic acid (SA) levels and SA-inducible *pathogenesis-related* (*PR*) transcripts (Nakashima et al., 2008; Li et al., 2010; Gallego-Giraldo et al., 2011a, 2011b; Lee et al., 2011; Van Acker et al., 2013). SA is a crucial phytohormone required for plant defense against pathogens (Vlot et al., 2009). The intriguing relationship between SA and lignin levels is mainly attributed to their biosynthetic overlap (Chen et al., 2009). There have been two major pathways proposed for SA biosynthesis in plants (Fig. 1). The initial pathway is derived from the shikimic acid pathway with isochorismate (Wildermuth et al., 2001). The secondary pathway through cinnamate involves a benzoate 2-hydroxylase (León et al., 1995). Theoretically, any flux modifications to the lignin pathway regulate the SA level. Alternatively, SA accumulation might result from the activation of endogenous defense responses by elicitor-active polysaccharides released from improperly lignified cell walls (Gallego-Giraldo et al., 2011a, 2011b).

[1]This work was supported by the National Key Research and Development Program of China (2018YFD1000300), the Earmarked Fund for China Agriculture Research System (CARS-27), and the Fundamental Research Funds for Central Universities (2452019049).

[2]These authors contributed equally to the article.

[3]Senior authors.

[4]Author for contact: fwm64@sina.com.

The author responsible for distribution of materials integral to the findings presented in this article in accordance with the policy described in the Instructions for Authors (www.plantphysiol.org) is: Fengwang Ma (fwm64@sina.com).

K.Z. and F.M. conceived the experiments; K.Z. and L.H. performed the experiments with assistance from Y.L., X.C., Z.Z., and B.L.; X.G. and P.L. contributed to discussion; K.Z. prepared the article; F.M. critically revised the article.

[OPEN]Articles can be viewed without a subscription.

www.plantphysiol.org/cgi/doi/10.1104/pp.19.00494

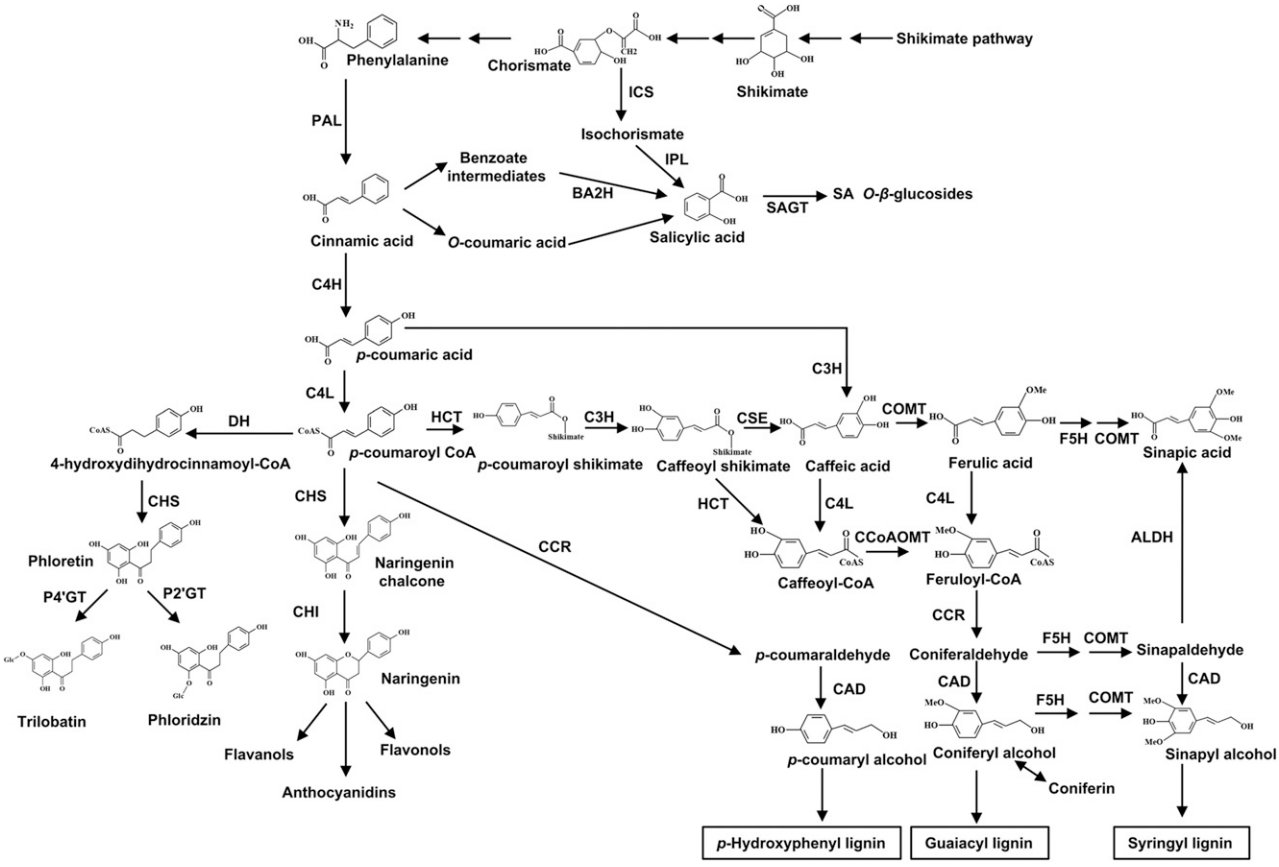

Figure 1. Biosynthetic pathways of SA, lignin, and phloridzin. ALDH, Aldehyde dehydrogenase; BA2H, benzoic acid-2-hydroxylase; CAD, cinnamyl alcohol dehydrogenase; CCR, cinnamoyl-coenzyme A reductase; C3H, C3-hydroxylase; C4H, cinnamate 4-hydroxylase; CHS, chalcone synthase; CHI, chalcone isomerase; 4CL, 4-coumarate:coenzyme A ligase; CoAOMT, caffeoyl-coenzyme A *O*-methyltransferase; COMT, caffeic acid *O*-methyltransferase; CSE, caffeoyl shikimate esterase; DH, dehydrogenase; F5H, ferulate 5-hydroxylase; HCT, hydroxycinnamoyl coenzyme A:shikimate hydroxycinnamoyl transferase; ICS, isochorismate synthase; IPL, isochorismate pyruvate lyase; PAL, phenylalanine ammonia lyase; P2′GT, UDP-glucose:phloretin 2′-*O*-glucosyltransferase; P4′GT, UDP-glucose:phloretin 4′-*O*-glucosyltransferase; SAGT, salicylic acid glucosyltransferase.

Dihydrochalcones (DHCs) are phenylpropanoids that are very similar to chalcones structurally, which are intermediates in flavonoid formation (Fig. 1). In apple (*Malus domestica*), phloridzin (phloretin 2′-*O*-glucoside), which is the predominant DHC, constitutes up to 90% of soluble phenolic compounds in young shoots and leaves (Gosch et al., 2009). This makes apple unique in the plant kingdom because phloridzin does not accumulate in such high amounts outside *Malus* spp. (Gosch et al., 2009). Variations in the DHC profile have been reported mostly within *Malus* spp., but little is known about their physiological relevance (Zhou et al., 2017, 2018; Gutierrez et al., 2018). Previous investigations reported that a *Valsa* canker-resistant apple, *Malus sieboldii*, accumulated less phloridzin than susceptible *M. domestica*. Moreover, the pathogen degraded phloridzin directly for the production of toxins [i.e. phloroglucinol, protocatechuic acid, *p*-hydroxybenzoic acid, 3-(*p*-hydroxyphenyl)propanoic acid, and *p*-hydroxyacetophenone] that facilitated necrosis in apple bark (Koganezawa and Sakuma, 1982; Natsume et al., 1982; Wang et al., 2014). Even so, there were no clear correlations between *Valsa* canker resistance and phloridzin levels (Bessho et al., 1994).

Valsa canker, which is caused predominantly by the necrotrophic fungus *Valsa mali*, is one of the most destructive diseases of apple in eastern Asia. Its successful infection only occurs in wounded plants, although the conidia of the pathogen can germinate on both wounded and intact bark. Infectious hyphae of *V. mali* can colonize, but not effectively degrade, xylem vessels (Yin et al., 2015). After they infect wounded tissues, the pathogen hyphae develop intercellularly and intracellularly and colonize all bark tissues, which results in severe tissue maceration and necrosis (Yin et al., 2015). Then, the infection causes twigs, limbs, or entire trees to die, and the infection can even cause entire orchards to fail (Ke et al., 2013). New lesions and infected trunks and shoots mostly appear in spring, and the canker develops rapidly between spring and early summer and then slowly after that (Abe et al., 2007). Because of its perennial nature and

the extensive penetration of its pathogen into host phloem and xylem, *Valsa* canker cannot be controlled effectively with agricultural chemicals (Yin et al., 2015). To date, microRNAs (Feng et al., 2017), pathogenic effectors (Zhang et al., 2018), toxic compounds (Natsume et al., 1982; Wang et al., 2014), and cell wall-degrading enzymes (Yin et al., 2015) have been implicated in the pathogenicity of *V. mali*. Previous work has shed light on the management of apple *Valsa* canker. Meanwhile, genetic engineering appears to be one of the most effective and practical methods to control this infection. However, there is very limited knowledge on *Valsa* canker resistance in apple.

As a side branch of the phenylpropanoid pathway, the biosynthesis of phloridzin is mediated by three successive steps: (1) NADPH-dependent formation of *p*-dihydrocoumaroyl-CoA from *p*-coumaroyl-CoA by dehydrogenase; (2) formation of phloretin from *p*-dihydrocoumaroyl-CoA and three molecules of malonyl-CoA by the common chalcone synthase (CHS); and (3) glycosylation of phloretin to phloridzin by UDP-glucose:phloretin 2′-*O*-glucosyltransferase (P2′GT; Fig. 1; Gosch et al., 2009, 2010). Previously, we identified a key P2′GT, MdUGT88F1, which converted phloretin into phloridzin directly in apple (Zhou et al., 2017). In this study, we analyzed comprehensively the physiological role of phloridzin using *MdUGT88F1* transgenic apple lines, which included overexpressing and silencing lines, and *Malus* spp. germplasm. Overall, our data clearly demonstrate that MdUGT88F1-mediated biosynthesis of phloridzin is critical for plant development and *Valsa* canker resistance by regulating the interplay between cell wall deposition and the accumulation of SA and reactive oxygen species (ROS) in apple trees.

RESULTS

Phloridzin Biosynthesis Is Vital to Apple Growth

We previously identified two P2′GTs, MdUGT88F1 and MdUGT88F4, that convert phloretin into phloridzin in apple (Zhou et al., 2017). In this study, the expression of the key *P2′GT* gene *MdUGT88F1* was modified preferentially using a transgenic method. As a result, we obtained four individual overexpressing (OE) lines and four individual RNA interference (RNAi) lines. Two pCambia2300-mediated OE lines, OE2-7 and OE3-4, and two pHellsgate2-mediated silencing lines, Ri-3 and Ri-6, all of which displayed altered expression levels, were selected (Supplemental Fig. S1). Slight phenotypic changes were only observed for Ri-3 and Ri-6 in tissue culture. Moreover, many phenotypic changes, which included severe stunting, reduced internode length, spindly leaf shape, more stems, and weak adventitious roots, were exhibited in RNAi apple lines when transplanted from tissue culture to the greenhouse (Fig. 2, A and B; Supplemental Table S1). Reverse transcription quantitative PCR (RT-qPCR) analysis showed that these phenotypic changes in RNAi apple lines were associated closely with reductions of *MdUGT88F1* and *MdUGT88F4* (Supplemental Fig. S1; Supplemental Table S2). Because the sequences of *MdUGT88F1* and *MdUGT88F4* are highly similar (Zhou et al., 2017), it was not possible to design primers to specifically

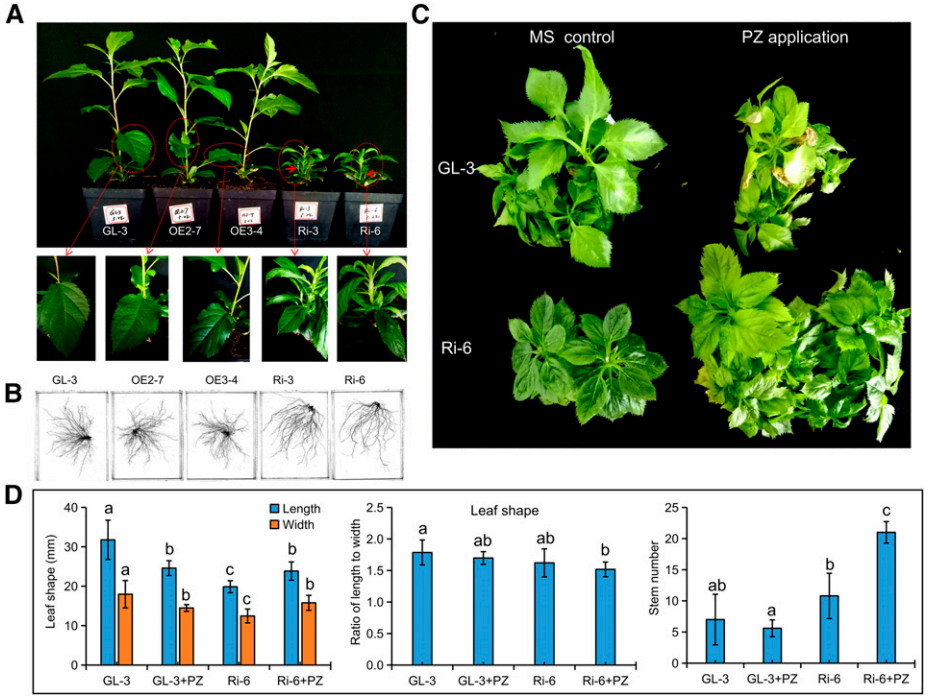

Figure 2. Decreased phloridzin biosynthesis resulted in severe reductions in growth in apple. A and B, Phenotypes of 38-d-old transgenic apple lines and GL-3. C and D, Assay of phloridzin compensation. Data are means ± SD ($n = 5$, five biological replicates). Values not represented by the same letter are significantly different ($P < 0.05$). MS control and PZ application represent normal and phloridzin-applied Murashige and Skoog (MS) regeneration medium, respectively.

knock down either *MdUGT88F1* or *MdUGT88F4* by RNAi. In contrast, OE2-7 and OE3-4 grew normally under both tissue-culture and greenhouse conditions (Fig. 2, A and B; Supplemental Table S1).

Analysis of the DHC profile revealed that there were no fluctuations observed in the OE apple lines (Table 1). In contrast, in the RNAi apple lines, phloridzin levels were largely reduced and trilobatin appeared to accumulate significantly, which suggested decreased P2′GT activity (Table 1). Moreover, under tissue-culture conditions, the application of phloridzin at 250 μM significantly alleviated the retardation of leaf development and promoted branching in Ri-6 but impeded the growth of GL-3 plantlets (Fig. 2, C and D), which suggested an enhanced phloridzin utilization efficiency in RNAi apple lines with reduced biosynthesis of phloridzin. Therefore, phloridzin biosynthesis is extremely vital to apple growth.

A Dwarf Phenotype Was Closely Associated with Reduced Lignin Accumulation in RNAi Apple Lines

Differences in growth increased between GL-3 and RNAi apple lines that were grown in greenhouse conditions for 3 months. Intriguingly, there was a higher root-shoot ratio (dry weight and length) in Ri-3 (Supplemental Fig. S2). Also, compared with those of GL-3, the thickened bark and reduced xylem in the stems of Ri-3 suggested a reduction of lignin (Fig. 3, A and B). Analysis of lignin verified that the cell wall residue (CWR) and acetyl bromide (AcBr) total lignin were reduced by 18.5% and 18.7%, respectively, in the stems of Ri-3 but not in roots (Fig. 3, C and D), which accounted for the higher root-shoot ratio.

Cellular organization of transgenic apple lines and GL-3 was examined by Toluidine Blue O staining (Fig. 4, A–D). Cross sections of leaves from Ri-3 revealed more compacted epidermal cells, a thicker palisade, and disorderly vascular bundles in the main veins compared with GL-3 (Fig. 4A). The spindly shape of RNAi apple leaves was associated mainly with a smaller angle between main and lateral veins, which reflected a disordered arrangement of the vascular bundle (Fig. 4, E and F). Cross sections of the stems of Ri-3 showed that reduced xylem coexisted with expanded phloem, parenchyma, and pith. The decreased xylem also resulted in vessels with smaller sizes and lower densities (Fig. 4B). In addition, there were compacted epidermal cells and parenchyma cells with different shapes in Ri-3 stems (Fig. 4, B and C). It is quite possible that these cellular changes made RNAi apple lines more resistant to *V. mali* (e.g. more compact cells may limit the spread of the pathogen). In contrast, there appeared to be no obvious leaf and stem changes in the OE apple lines (Fig. 4, A and B). Vascular bundles of the transgenic and nontransgenic apple roots were basically similar in morphology (Fig. 4D). GUS staining showed that there was obvious GUS activity in the stem vascular bundles of lines expressing *ProMdUGT88F1*:*GUS* but not in an Arabidopsis (*Arabidopsis thaliana*) line expressing *ProMdUGT88F4*:*GUS* (Supplemental Fig. S3), which supported the hypothesis that MdUGT88F1-mediated phloridzin biosynthesis plays an important role in the development of stem vascular bundles. Indeed, Gaucher et al. (2013b) also found that DHCs localized around the vascular system in apple.

Results from Wiesner and Mäule staining further confirmed that there was less lignin or fewer cells that contained lignin (i.e. a smaller xylem region in RNAi apple stems; Fig. 4, G and H). Metabolic analysis revealed that *p*-coumaric acid and hydroxycinnamoyl derivatives were greatly reduced in RNAi apple leaves (Supplemental Table S3). Among these decreased derivatives, *p*-coumaryl alcohol and sinapaldehyde participate directly in the biosynthesis of H- and S-lignin, respectively. However, there were no differences among the precursors of G-lignin, which include coniferaldehyde and coniferyl alcohol. Taken together, the dwarf phenotype of the RNAi apple lines was closely associated with reduced lignin accumulation.

Abnormal Composition of Cell Wall Polysaccharides Mediated by Myoinositol Metabolism Contributed Partly to Growth Reduction in RNAi Apple Lines

Theoretically, UDP-Glc fluctuations resulted in changes in sugar metabolism in phloridzin biosynthesis-decreased RNAi apple lines. Metabolic analysis showed that the

Table 1. *DHC profiles of transgenic apple lines and GL-3 ($\mu g\ g^{-1}$ fresh weight)*

Data are means ± SD ($n = 3$, three biological replicates). ***, $P < 0.001$; **, $P < 0.01$; nd, not determined.

Tissues	DHCs	GL-3	OE2-7	OE3-4	Ri-3	Ri-6
Leaf	Phloridzin	14,731.75 ± 488.89	14,902.97 ± 314.81	14,753.02 ± 620.25	8,029.11 ± 643.45***	6,125.08 ± 341.55***
	Trilobatin	nd	nd	nd	152.81 ± 10.26	125.75 ± 9.69
	Phloretin	107.42 ± 43.58	123.09 ± 29.56	129.74 ± 30.6	145.73 ± 29.96	83.28 ± 10.33
Stem	Phloridzin	8,308.29 ± 333.41	8,213.76 ± 391.2	8,071.4 ± 379.38	4,704.85 ± 386.23***	5,052.73 ± 722.73**
	Trilobatin	nd	nd	nd	100.17 ± 9.29	143.24 ± 14.79
	Phloretin	nd	nd	nd	nd	nd
Root	Phloridzin	6,475.3 ± 355.73	6,565.33 ± 1,284.84	6,497.38 ± 403.82	2,117.73 ± 309.18***	2,280.12 ± 277.35***
	Trilobatin	nd	nd	nd	68.91 ± 15.8	79.98 ± 10.89
	Phloretin	nd	nd	nd	nd	nd

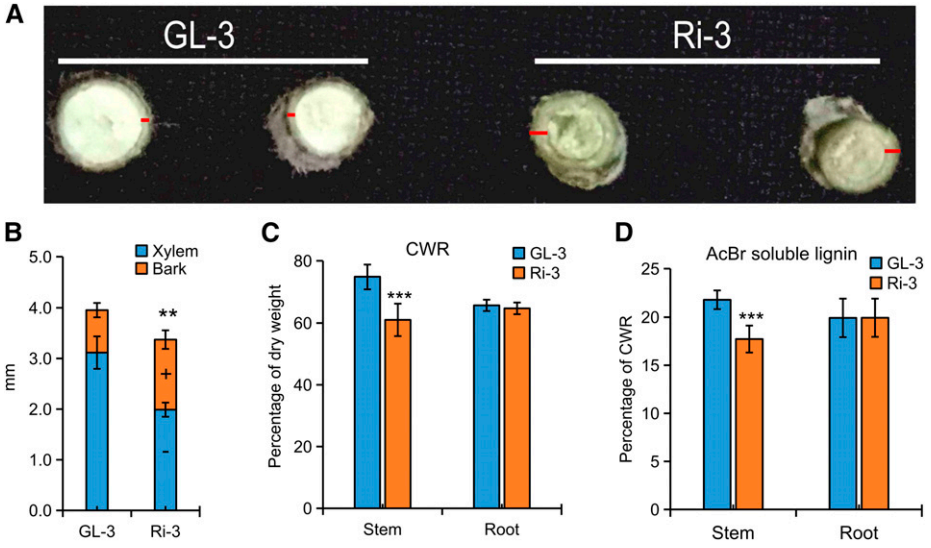

Figure 3. Down-regulation of phloridzin biosynthesis decreased lignin accumulation in apple. A and B, Stem compositions in 3-month-old GL-3 and Ri-3. C and D, CWR content (C) and AcBr total lignin concentration (D) in the stems and roots of GL-3 and Ri-3. Bark was marked with red lines. Data are means ± SD ($n = 5$ for B, five plants were used for each line; $n = 5$ for C, five biological replicates; $n = 10$ for D, 10 biological replicates). In comparison with GL-3, ***, $P < 0.001$ and **, $P < 0.01$. + and − indicate significant increases and decreases, respectively ($P < 0.05$).

levels of Glc and myoinositol decreased significantly in RNAi apple leaves, where values were 46% to 58% and 45% to 61% of those measured in GL-3, respectively (Supplemental Table S3). Such reductions were further verified by gas chromatography-mass spectrometry analysis. For Glc, there appeared to be a slight increment in OE apple stems. However, there were significant reductions found in both leaves and stems of RNAi apple lines (Fig. 5A). There were no differences among myoinositol levels found in leaves or stems of OE apple lines. In contrast, myoinositol levels decreased in leaves and, in particular, stems of RNAi apple lines (Fig. 5B).

To test if myoinositol reduction partly accounted for the stunted growth observed in RNAi apple lines, we conducted a myoinositol depletion assay. Under MS control conditions, leaf shapes of OE2-7, Ri-6, and GL-3 were basically the same. However, under

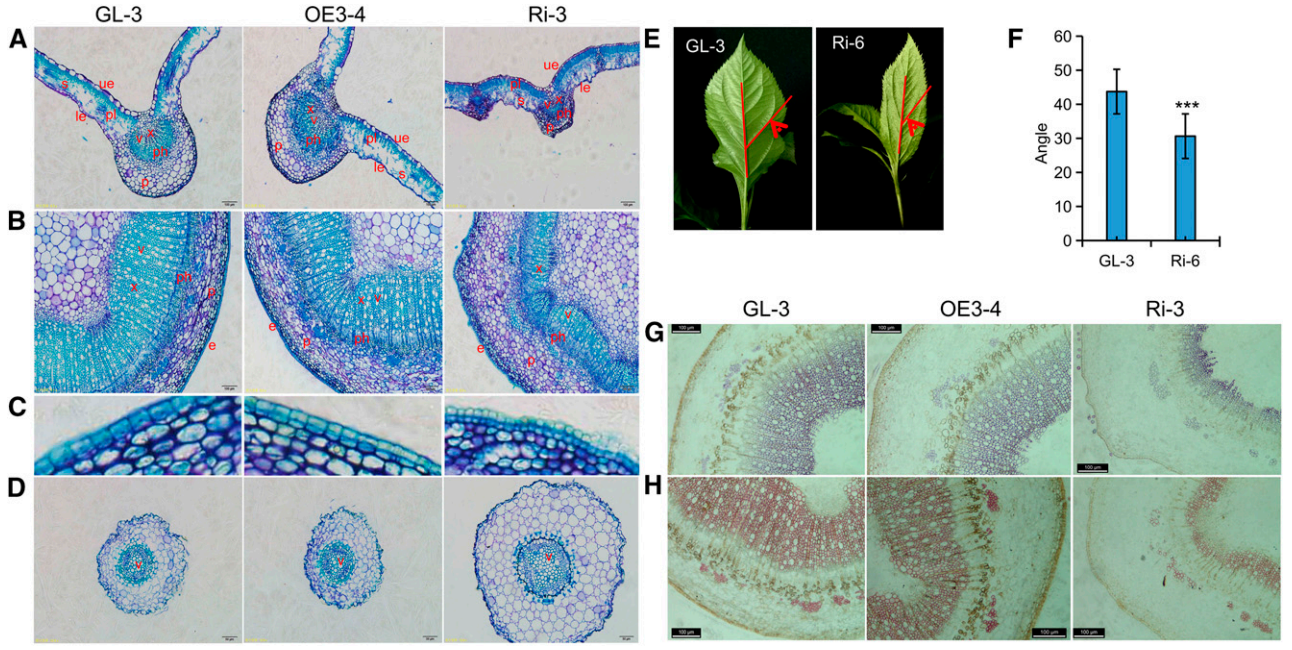

Figure 4. Histochemical and morphological analyses of transgenic apple lines. A, B, and D, Toluidine Blue O staining of cross sections of a leaf (A), stem (B), and root (D) of GL-3 and transgenic apple lines. C, Higher magnification of a portion of the stem highlighting the epidermal cells. E and F, Angles between main and lateral veins of the leaves of GL-3 and Ri-6. G and H, Wiesner (G) and Mäule (H) staining of the stem cross sections of GL-3 and transgenic apple lines. Data are means ± SD ($n = 11$, 11 leaves from 11 plants were used for each line). Asterisks in F indicate a significant difference from GL-3 at $P < 0.001$. le, lower epidermis; p, parenchyma; ph, phloem; pl, palisade cells; s, spongy mesophyll; ue, upper epidermis; v, vessel; x, xylem. Bars = 100 μm (A, B, G, and H) and 50 μm (D).

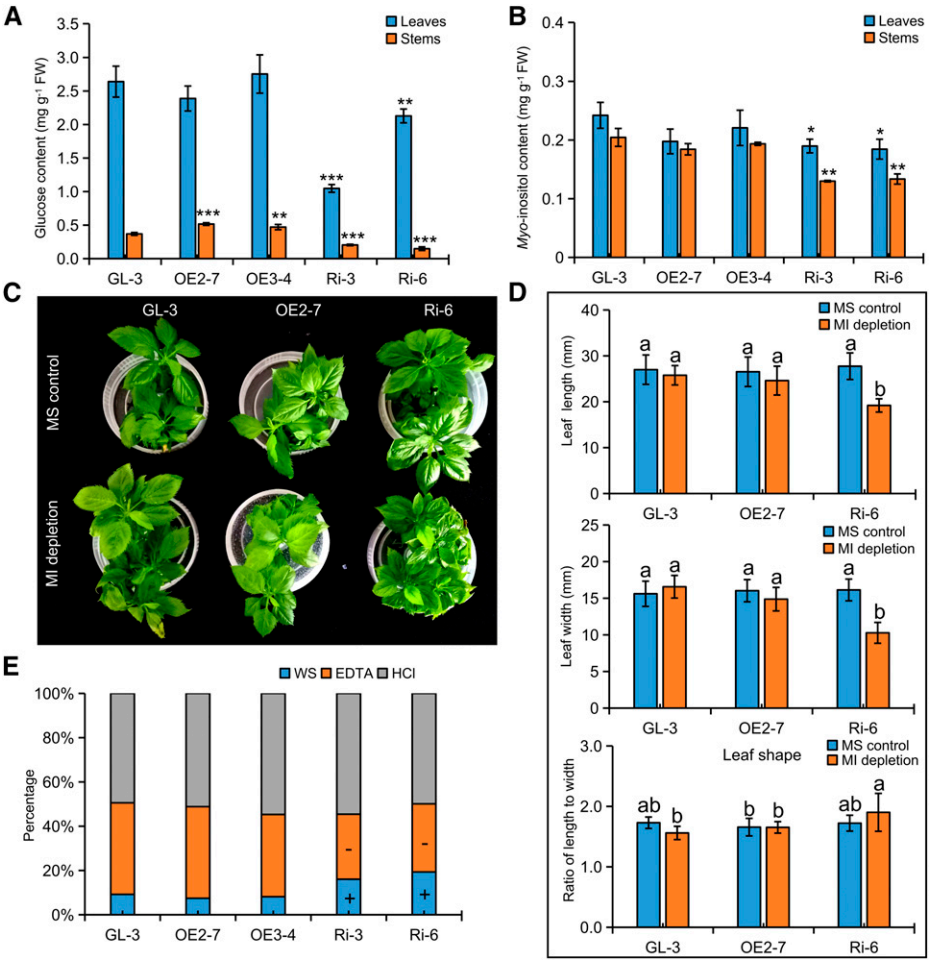

Figure 5. Decreased phloridzin biosynthesis resulted in disorders in myoinositol metabolism and cell wall polysaccharides. A and B, Levels of Glc (A) and myoinositol (B) in the leaves of the 38-d-old transgenic apple lines and GL-3. FW, Fresh weight. C and D, Assay results of myoinositol depletions. E, Compositions of pectic materials in stems of the 38-d-old transgenic apple lines and GL-3. Data are means ± SD ($n = 3$ for A, B, and E, three biological replicates; $n \geq 7$ for D, at least seven biological replicates). In comparison with GL-3, ***, $P < 0.001$; **, $P < 0.01$; and *, $P < 0.05$. Values not represented by the same letter are significantly different ($P < 0.05$). + and − indicate significant increases and decreases, respectively ($P < 0.05$). MS control and MI depletion represent normal and myoinositol-depleted MS regeneration medium, respectively; WS, EDTA, and HCl represent crude cold water, EDTA, and HCl soluble fractions, respectively.

myoinositol-depleted conditions, stunted leaf growth occurred only in Ri-6, which indicated that the dwarf phenotype may be related to myoinositol reduction in RNAi apple lines (Fig. 5, C and D). RNA sequencing (RNA-seq) analysis also revealed that two *Galactinol synthase* (*GolS*) genes were highly upregulated in RNAi apple leaves (Supplemental Table S2). In Arabidopsis, GolS enzyme directly converted myoinositol into galactinol for the biosynthesis of raffinose-family oligosaccharides, and it affected the composition of cell wall polysaccharides indirectly (Valluru and Van den Ende, 2011). Because there were Glc and myoinositol reductions in the RNAi apple lines, we analyzed cell wall polysaccharides in the stems of transgenic apple lines and GL-3. Levels of cellulose and total pectic materials were essentially the same in transgenic and nontransgenic apple plants (Supplemental Fig. S4), but different pectic compositions were found in both Ri-3 and Ri-6. The cold water-soluble (WS) pectins increased at the expense of the EDTA-soluble pectic materials (Fig. 5E). Thus, the decreased biosynthesis of phloridzin probably disturbed the composition of cell wall polysaccharides through myoinositol metabolism in RNAi apple lines.

Decreased Biosynthesis of Phloridzin Significantly Enhanced Resistance to *V. mali* in RNAi Apple Lines

Previous studies suggested that phloridzin might increase susceptibility to *Valsa* canker in apple (Koganezawa and Sakuma, 1982; Bessho et al., 1994). Accordingly, transgenic and nontransgenic apple leaves (Fig. 6, A and C) and stems (Fig. 6, B and D) were inoculated with *V. mali*. Three days after inoculation, lesions were observably smaller in RNAi apple lines and slightly larger in OE apple lines compared with GL-3. Also, RT-qPCR showed that OE apple lines and GL-3 responded to infection by downregulating *MdUGT88F1* and *MdUGT88F4* (Fig. 6, E and F). However, it is very difficult to assess the transcriptomic effects of *V. mali* on *MdUGT88F1* when RNAi apple lines were also being actively silenced for this gene (Fig. 6, E and F). Meanwhile, in leaves of GL-3, phloridzin was reduced significantly by *V. mali*. But a relatively lower reduction led to a higher phloridzin accumulation in OE apple leaves after *V. mali* infection. Yet, there were very small changes following infection in RNAi apple leaves (Fig. 6G), although there still appeared to be a reduction in trilobatin (Fig. 6H). Phloretin was reduced in the leaves of RNAi

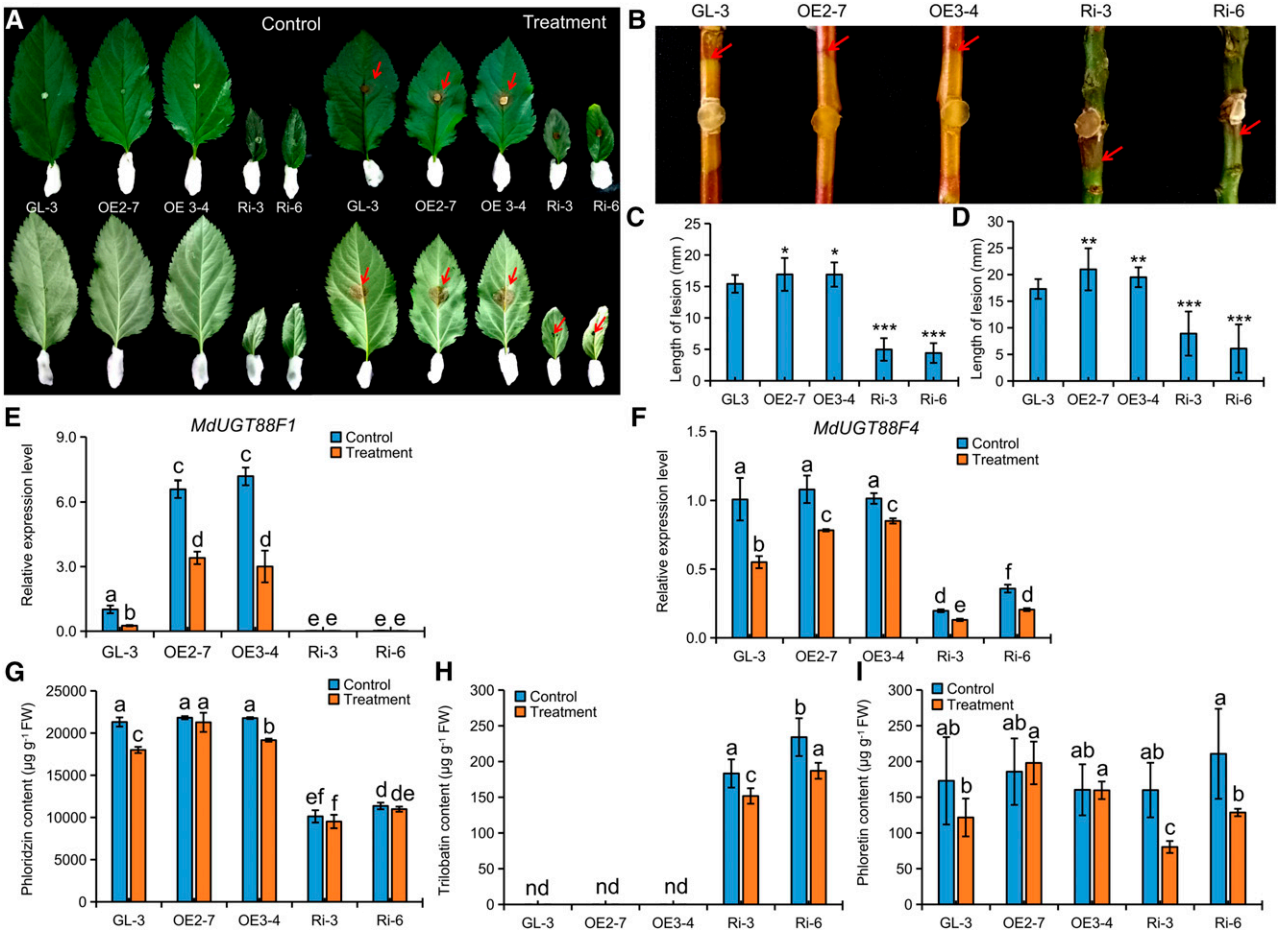

Figure 6. Down-regulation of *MdUGT88F1* resulted in enhanced resistance to *V. mali* infection. A to D, Evaluation results of *Valsa* canker resistance in the transgenic apple lines and GL-3 by leaf (A and C) and stem (B and D) inoculation. E to I, Changes of *MdUGT88F1* (E) and *MdUGT88F4* (F) expression and DHC levels (G–I) in the leaves of transgenic apple lines and GL-3 in response to *V. mali* infection. FW, Fresh weight. Data are means ± SD ($n \geq 15$ for C and D, at least 15 plants [one leaf or stem from each plant] were used for each line; $n = 3$ for E–I, three biological replicates). In comparison with GL-3, ***, $P < 0.001$; **, $P < 0.01$; and *, $P < 0.05$. Values not represented by the same letter are significantly different ($P < 0.05$). Control, Potato dextrose agar (PDA) control; nd, not determined; Treatment, *V. mali*-infected leaves.

apple lines but was unchanged in both GL-3 and OE apple leaves (Fig. 6I). Thus, MdUGT88F1-mediated phloridzin biosynthesis appeared to have a negative effect on *Valsa* canker resistance in apple.

Phloridzin Was Utilized Directly as a Sugar Alternative and a Toxin Accelerator by *V. mali*

To elucidate the mechanism of phloridzin in resistance to *Valsa* canker, the correlation between bark phloridzin levels and *Valsa* canker resistance in *Malus* spp. was investigated based on our previous investigation (Zhou et al., 2017; Supplemental Table S4). Although there were no significant correlations found, we observed a connection between *Valsa* canker susceptibility and an increase in DHC content (Supplemental Fig. S5A). Next, two *Malus* spp. accessions that displayed contrasting susceptibilities to *V. mali* (i.e. susceptible and higher-DHC apple ZD1 [*Malus hupehensis*] compared with a lower-DHC and resistant apple ZH16 [*Malus toringo*]) were selected for further analysis (Supplemental Fig. S5, B and C). In ZD1, a decrease in DHC-glucosides and an increase in aglycone phloretin indicated that deglycosylation of DHC-glucosides occurred in response to *V. mali* invasion. In ZH16, there was a similar trend for DHCs upon infection with *V. mali*, although there were no significant differences (Supplemental Fig. S5D). Furthermore, β-glucosidase activity in the infected bark increased gradually in both ZD1 and ZH16 (Supplemental Fig. S5E). Both phloridzin and phloretin were characterized by a weakly antimicrobial property toward *V. mali* (Supplemental Fig. S6). However, phloridzin (0.5 mM) remained favorable for *V. mali* growth. We observed accelerated deglycosylation of phloridzin followed by rapid degradation of phloretin once Glc was depleted in lines inoculated

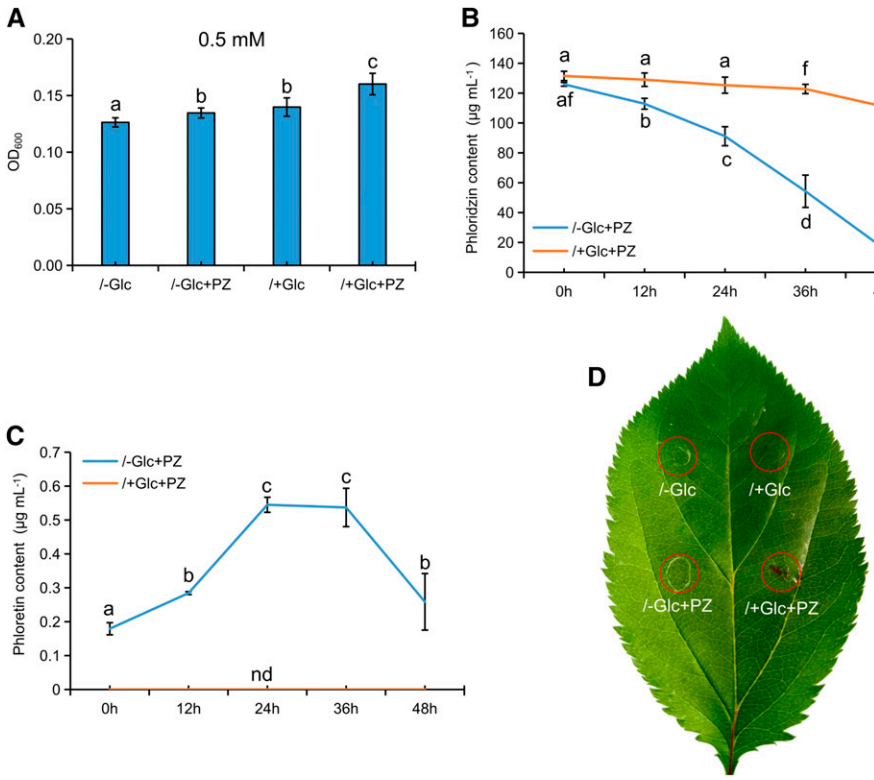

Figure 7. Phloridzin directly promotes growth and toxin production of *V. mali*. A, Effects of phloridzin on *V. mali* growth after 48 h of culture. B and C, Change in phloridzin (B) and phloretin (C) concentration in culture. nd, not determined. D, Assay of toxins from the 48-h culture residues. /+Glc, Normal PDB; /−Glc, PDB without Glc; /+Glc+PZ, normal PDB with phloridzin added (0.5 mM); /−Glc+PZ, PDB without Glc and with phloridzin added (0.5 mM). Data are means ± SD ($n = 4$, four biological replicates). Values not represented by the same letter are significantly different ($P < 0.05$).

with *V. mali* (Fig. 7, A–C; Supplemental Fig. S6, C and D). Thus, we concluded that *V. mali* hydrolyzed phloridzin and consumed Glc by releasing β-glucosidase in barren apple bark. Additionally, 48 h after incubation of *V. mali*, only the residual liquid from phloridzin-added normal potato dextrose broth (PDB) caused obvious necrosis in apple leaves (Fig. 7D). Thus, it appeared that phloridzin also accelerated tissue necrosis by facilitating the production of toxins by *V. mali* (Fig. 7).

Gene expression analysis showed that *UGT88F1* and *UGT88F4* were down-regulated in both ZD1 and ZH16 apple bark after infection by *V. mali*, although both *PAL* and *CHS* were induced (Supplemental Fig. S7). Generally, plants employ multiple mechanisms to protect themselves from pathogen infection. The down-regulated expression of *UGT88F1* in both resistant and susceptible apples reflected a common involvement of phloridzin in *Valsa* canker resistance. Moreover, the negative involvement of phloridzin was also verified in transgenic apple lines. Thus, the MdUGT88F1-mediated phloridzin biosynthesis would be one of the factors that determined resistance to *Valsa* canker in apple trees. That is, phloridzin was utilized directly as a sugar alternative and a toxin accelerator for *V. mali* in apple.

Levels of SA and ROS Are Implicated in *Valsa* Canker Resistance in Apple

RNA-seq analysis revealed that a large number of genes involved in plant-pathogen interactions (e.g. *PR* genes and SA biosynthesis regulatory genes) were largely induced in RNAi apple leaves (Supplemental Table S2). RT-qPCR demonstrated that the expression of *MdPR1*, *MdPR2*, *MdPR4*, *MdPR5*, and *MdPR8* was largely up-regulated in RNAi apple leaves but remained unchanged in OE apple leaves (Supplemental Fig. S8A). Phytohormone analysis verified that both free SA and total SA were largely accumulated in RNAi apple leaves, but only total SA was reduced slightly in OE3-4 leaves (Fig. 8, A and B). Moreover, these *PRs* were differentially up-regulated in leaves from transgenic apple lines and GL-3 in response to *V. mali* infection (Fig. 8D). Compared with GL-3, higher expression was still shown in RNAi apple lines, but in OE apple lines, lower levels of *MdPR1* and *MdPR2* and similar accumulation of *MdPR4*, *MdPR5*, and *MdPR8* were found (Fig. 8D). The up-regulated *PR* genes (Supplemental Fig. S8B) and increased SA levels (Fig. 8C) in both ZD1 and ZH16 upon infection with *V. mali* suggested a positive role of SA in *Valsa* canker resistance in apple.

DHCs are considered to be excellent antioxidant compounds (Dugé de Bernonville et al., 2010; Xiao et al., 2017). In particular, the large reductions in phloridzin (Table 1) and hydroxycinnamoyl derivatives (Supplemental Table S3) certainly would interfere with the redox state in RNAi apple lines. Staining with nitroblue tetrazolium (NBT) and diaminobenzidine (DAB) revealed a strong increase in hydrogen peroxide (H_2O_2) and superoxide ion (O_2^-) accumulation in leaves of RNAi lines when compared with those of GL-3, although there were no significant differences in leaves of OE lines (Fig. 9A).

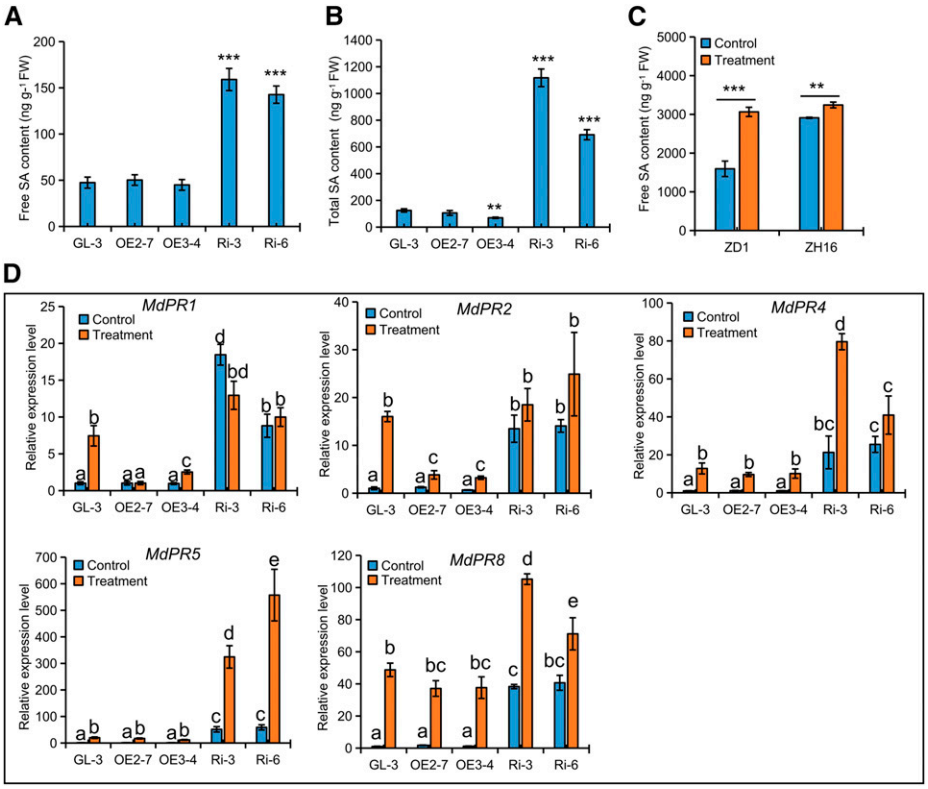

Figure 8. SA is positively implicated in *Valsa* canker resistance in RNAi lines. A and B, Levels of free (A) and total (B) SA in the leaves from 38-d-old transgenic apple lines and GL-3. C, Free SA levels of susceptible ZD1 and resistant ZH16 apple bark on day 4 after their infection by *V. mali*. FW, Fresh weight. D, Expression changes in *MdPR* genes in the leaves of transgenic apple lines and GL-3 in response to *V. mali* infection. Data are means ± SD ($n = 3$, three biological replicates). In comparison with GL-3 or control, ***, $P < 0.001$ and **, $P < 0.01$. Values not represented by the same letter are significantly different ($P < 0.05$). Control, PDA control; Treatment, *V. mali*-infected bark (C) or leaves (D).

In addition, metabolic analysis showed that levels of oxidized and reduced glutathione decreased in RNAi apple leaves to approximately 28% and 25%, respectively, of those measured in GL-3. Also, there was a slight reduction in L-ascorbate (Supplemental Table S3). Such reductions largely accounted for the high ROS accumulation in RNAi apple lines. Moreover, H_2O_2 was differentially induced in transgenic and nontransgenic apple leaves after infection by *V. mali*. (Fig. 9B). Although there were no differences between GL-3 and OE lines under controlled conditions, lower induction levels resulted in lower H_2O_2 accumulation in both OE lines upon infection with *V. mali*. In contrast, rare inductions resulted in comparable H_2O_2 levels in GL-3 and RNAi apple leaves (Fig. 9B), which suggested that a higher prechallenge level of H_2O_2 was important (Fig. 9, C and D). In addition, in susceptible ZD1, H_2O_2 decreased gradually after infection by *V. mali* (Fig. 9C). However, in resistant ZH16, H_2O_2 was induced rapidly and remained at a relatively higher level (Fig. 9D). This indicated that ROS levels played a key role in *Valsa* canker resistance in apple. In summary, after pathogen infection, decreased phloridzin biosynthesis increased the levels of SA and ROS, which enhanced *Valsa* canker resistance in apple.

DISCUSSION

Phloridzin appears to play important physiological roles in plant development and pathogen defense in apple (Zhang et al., 2007; Dare et al., 2013; Hutabarat et al., 2016). In this study, we used *MdUGT88F1*, the key *P2′GT* gene, transgenic apple lines, and wild *Malus* spp. accessions to gain new insight into the functions of phloridzin in apple. Overall, our results provided insight into the importance of MdUGT88F1-mediated phloridzin biosynthesis in the interplay between plant development and pathogen resistance in apple trees.

We observed a severe reduction in growth in the MdUGT88F1-RNAi apple lines with decreased phloridzin biosynthesis. Other researchers also reported a very similar phenotype in *UGT88F1* silencing lines (Dare et al., 2017). Results from Dare et al. (2017) and this study revealed the presence of trilobatin in the *MdUGT88F1* silencing lines, which indicated that decreased P2′GT activity led to a higher conversion of phloretin to trilobatin by UDP-glucose:phloretin 4′-*O*-glucosyltransferase (P4′GT). Interestingly, a *P4′GT* gene, *MdPh-4′-OGT*, was previously identified and found to be expressed in 'Golden Delicious' apple, which does not accumulate trilobatin (Yahyaa et al., 2016). Independent silencing of *CHS* and *UGT88F1* also resulted in similar phenotypes in apple (Dare and Hellens, 2013; Dare et al., 2013, 2017). However, such phenotypic changes were not found in CHS null mutants from Arabidopsis, a species that lacks phloridzin accumulation (Shirley et al., 1995; Li et al., 2010). Thus, these results collectively indicated that decreased biosynthesis of phloridzin caused stunted growth in *MdUGT88F1* silencing lines, which was verified further

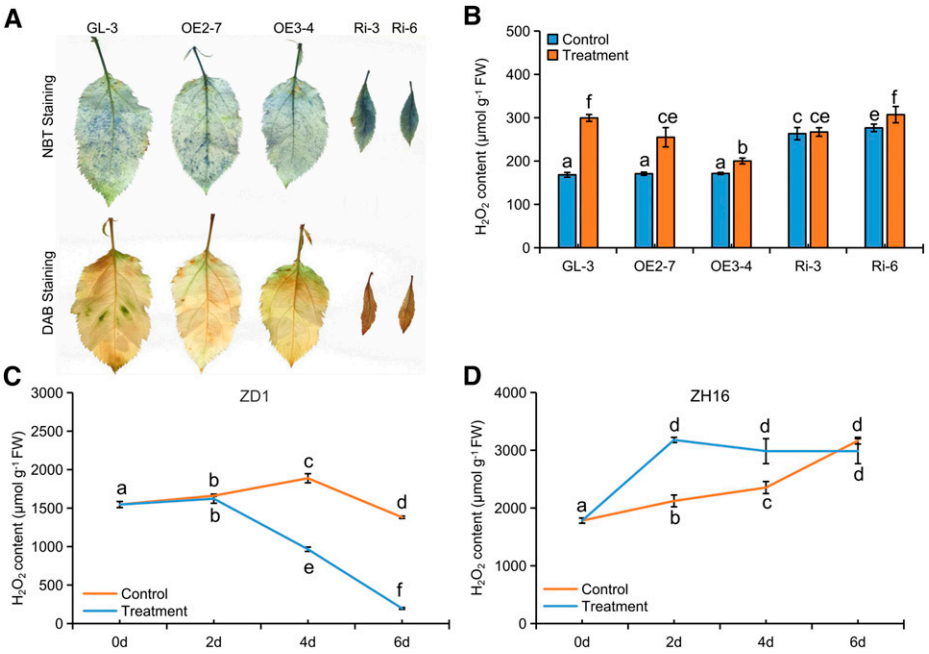

Figure 9. Increased ROS accumulation contributed to enhanced *Valsa* canker resistance in RNAi lines. A, NBT and DAB staining of the leaves of transgenic apple lines and GL-3. B, Changes in concentration of H_2O_2 in the leaves from transgenic apple lines and GL-3 in response to *V. mali* infection. C and D, Changes in concentration of H_2O_2 in susceptible apple ZD1 (C) and resistant apple ZH16 (D) in response to *V. mali* infection. Data are means ± SD ($n = 3$, three biological replicates). Values not represented by the same letter are significantly different ($P < 0.05$). Control, PDA control; FW, fresh weight; Treatment, *V. mali*-infected leaves (B) or bark (C and D).

by our study and Dare et al. (2017), who used a phloridzin compensation assay.

Dwarf phenotypes in both *CHS* and *UGT88F1* silencing lines were attributed to increased auxin transport, but flavonoids were also changed substantially (Dare et al., 2013, 2017). Flavonoids are regarded by many to be key modulators of auxin transport (Besseau et al., 2007), but there are also reports that seem to contradict this belief (Li et al., 2010; Gallego-Giraldo et al., 2011b). Even so, this does not exclude the possible involvement of auxin in the plant development of *MdUGT88F1* silencing lines. Our data confirmed that phloridzin was a critical compound in modulating the phenylpropanoid pathway flux. Lignin is a major structural component of the secondary cell wall, and transgenic plants impaired in lignin biosynthesis frequently exhibit reductions in growth (Li et al., 2010; Gallego-Giraldo et al., 2011b).

In this study, we compared our results carefully with other knockout lines affected in the lignin pathway (Van Acker et al., 2013). Although the decrease in AcBr soluble lignin was comparable with other lignin-reduced plants, the decrease of CWR was very severe. Eventually, both led to an approximately 35% reduction in total lignin in MdUGT88F1-RNAi lines, which represented an appreciable reduction. Also, hydroxycinnamoyl derivatives were reduced significantly in MdUGT88F1-RNAi lines. Decreased levels of *p*-coumaryl alcohol and sinapaldehyde ultimately resulted in large losses of lignin and stunted growth. Moreover, down-regulation was identified in nine of the 11 differentially expressed *Laccase* genes in MdUGT88F1-RNAi lines (Supplemental Table S2). In addition to peroxidase, laccases are also necessary for lignin polymerization through the oxidative polymerization of monolignols (Sun et al., 2018). Consistent with this, down-regulation of *UGT88F1* also resulted in large reductions of hydroxycinnamoyl derivatives and a smaller stem xylem region (Dare et al., 2017). In addition, a metabolome and RNA-seq analysis revealed that increased expression of *GolS* and decreased Glc levels were likely responsible for the myoinositol reduction in MdUGT88F1-RNAi lines (Valluru and Van den Ende, 2011). After myoinositol was depleted, a strong reduction in growth was observed in MdUGT88F1-RNAi lines. Moreover, the myoinositol reduction was accompanied by modifications of pectic materials. As a versatile compound, myoinositol is essential for plant growth (Cui et al., 2013; Ye et al., 2016) and is involved in the production of cell wall polysaccharides (Valluru and Van den Ende, 2011). Thus, the severely dwarfed phenotype among the MdUGT88F1-RNAi apple lines with decreased phloridzin biosynthesis was related closely to interference with cell wall deposition (i.e. decreased lignin levels and disorders of cell wall polysaccharides).

SA was previously shown to cause reduced growth of plants with down-regulated lignin (Gallego-Giraldo et al., 2011a, 2011b). In *MdUGT88F1* silencing lines, decreased *p*-coumaric acid and stable cinnamic acid levels indicated enhanced metabolic flux into SA biosynthesis (Supplemental Table S3). Along with increased SA levels, the SA marker genes *PRs* and the SA biosynthesis regulatory genes *ENHANCED DISEASE SUSCEPTIBILITY1* and *PHYTOALEXIN DEFICIENT4* were also induced substantially in MdUGT88F1-RNAi lines (Supplemental Table S2). Also, the release of pectic elicitors from underlignified secondary cell walls in lignin-reduced plants induced SA accumulation (Gallego-Giraldo et al., 2011a, 2011b). Consistently, the

WS-pectic materials increased at the expense of EDTA-pectins in MdUGT88F1-RNAi lines. This modification was verified by decreased myoinositol, which is a key precursor of cell wall polysaccharides. A decrease in myoinositol was previously shown to trigger SA-dependent programmed cell death (PCD) in plants (Chaouch and Noctor, 2010; Bruggeman et al., 2015). Thus, it was likely that increased SA levels were attributed to spillover from the phenylpropanoid pathway and myoinositol-dependent release of pectic elicitors in MdUGT88F1-RNAi apple lines.

Our study also suggested that in MdUGT88F1-RNAi lines, decreased phloridzin biosynthesis enhanced *Valsa* canker resistance by increasing the SA level through indirect modulation of cell wall deposition. SA signaling predominantly combats biotrophic pathogens and viruses, whereas jasmonic acid (JA) signaling is critical for the response to necrotrophic pathogens and insects (Glazebrook, 2005; Vlot et al., 2009). Generally, *V. mali* is considered to be a necrotrophic pathogen (Yin et al., 2015). However, *Valsa* canker resistance would be independent of JA in transgenic apple lines (Supplemental Fig. S9A). The role of SA in plant defense is frequently associated with the accumulation of ROS and the activation of diverse groups of defense-related genes, which mediate a hypersensitive response (a fast PCD; Apel and Hirt, 2004; Vlot et al., 2009; Daudi et al., 2012). PCD is believed to be detrimental to biotrophic and hemibiotrophic pathogens, because of a reduction of vivosphere and restriction of hyphae extension, but beneficial to infections caused by necrotrophic pathogens (Gilchrist, 1998). Here, we revealed a positive potential of SA in *Valsa* canker resistance in apple. Similarly, Yin et al. (2016a) found that genes involved in apple SA signaling were significantly up-regulated after *V. mali* infection. To counteract SA-induced defense responses, *V. mali* may have acquired a salicylate hydroxylase gene (which encodes an enzyme that degrades SA) through horizontal gene transfer from bacteria (Tanaka et al., 2015; Yin et al., 2016b).

In MdUGT88F1-RNAi lines, there were higher pre-challenge levels of ROS, although little induction of H_2O_2 was identified upon infection with *V. mali*. Increased ROS levels were attributed mainly to a compromised antioxidant system, which included decreases in phloridzin, hydroxycinnamoyl derivatives, oxidized glutathione, reduced glutathione, and L-ascorbate (Wang et al., 2012). Furthermore, the contrasting H_2O_2 dynamics in susceptible ZD1 and resistant ZH16 lines indicated that oxidative burst may be a key

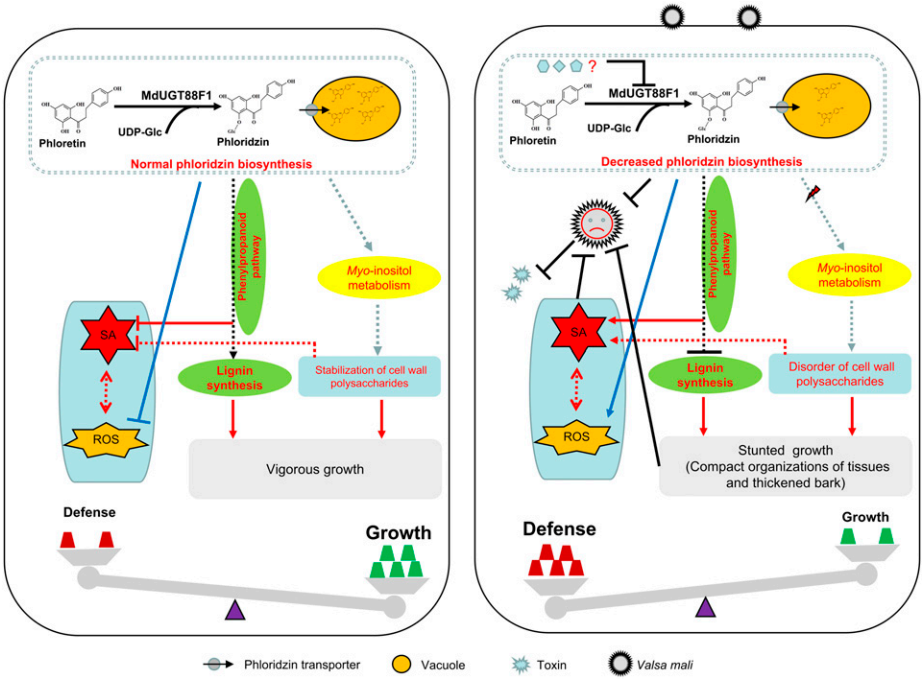

Figure 10. A model for MdUGT88F1-mediated phloridzin biosynthesis regulating plant development and *Valsa* canker resistance in apple. In nature, normal phloridzin biosynthesis maintains well-balanced cell wall deposition and supports vigorous growth in apple. After infection by *V. mali*, MdUGT88F1-mediated phloridzin biosynthesis is decreased through an unknown mechanism, which causes lignin reduction and SA accumulation by indirectly changing phenylpropanoid pathway flux. In addition, decreased phloridzin biosynthesis gives rise to disorders of cell wall polysaccharides by indirectly changing myoinositol metabolism, which also stimulates the accumulation of SA. Modified cell wall deposition results in growth reduction but also reinforcement of tissue. The reinforced tissue inhibits infection by *V. mali* along with increases in SA and ROS. Also, decreased phloridzin biosynthesis directly delays growth and toxin production of *V. mali* and promotes accumulation of ROS. Eventually, apple trees adjust to *V. mali* infection. Solid and dashed lines refer to direct and indirect effects, respectively.

factor for *Valsa* canker resistance in apple. It has been observed previously that H_2O_2 can induce the accumulation of SA and vice versa (Guo et al., 2017). In susceptible ZD1, the loss of key modulator(s) in the positive feedback loop of SA and ROS made it necessary to investigate further the role of ROS in *Valsa* canker resistance in apple.

ROS act as antimicrobial molecules and are important signals that mediate plant disease resistance. However, excessive ROS can be phytotoxic (Suzuki et al., 2011). Necrotrophs are defined as pathogens that derive energy from dying or dead plant tissues, but they differ substantially in the progression of pathogenesis, ranging from rapidly killing host cells, such as *Botrytis cinerea*, to having an extended asymptomatic phase before killing host cells, such as *Alternaria alternata* (Oliver et al., 2012; Meng et al., 2018). Recently, it was suggested that suppressing PCD probably played an important role in infections by *V. mali*. *V. mali* may not need to kill host cells rapidly but instead may regulate their death to enable successful colonization over time (Zhang et al., 2018). In this study, we showed that JA does not appear to be involved in *Valsa* canker resistance in apple (Supplemental Fig. S9, B and C). We speculated that *V. mali* could be a heminecrotrophic or hemibiotrophic pathogen.

We also considered that phloridzin may be utilized directly as a sugar alternative and a toxin accelerator by *V. mali* in apple. Large quantities of Glc from the internal stock of phloridzin released by the action of β-glucosidase might act as a complementary source of carbohydrates and favor the fast multiplication of *V. mali*. A similar case was characterized in fire blight (*Erwinia amylovora*; Gaucher et al., 2013a). In that case, the aglycone phloretin from phloridzin deglycosylation was degraded rapidly into toxins by *V. mali*, which facilitated the establishment of infection and lesion expansion (Koganezawa and Sakuma, 1982; Natsume et al., 1982; Wang et al., 2014). We also found that phloridzin may facilitate toxin production by *V. mali* through signaling pathways rather than acting simply as metabolites for toxin production. Meanwhile, upon infection with *V. mali*, apple optimized its *Valsa* canker response through self-regulation. Down-regulation of *UGT88F1* and *UGT88F4* was identified in both susceptible ZD1 and resistant ZH16 after infection, although both *PAL* and *CHS* were induced. We verified that a higher level of phloridzin compromised *Valsa* canker resistance slightly in MdUGT88F1-OE apple lines following *V. mali* infection. In contrast, in MdUGT88F1-RNAi apple lines, decreased phloridzin biosynthesis and lower Glc levels limited the growth and infection of *V. mali* directly. In addition, the tightly organized tissues (e.g. compact epidermis and thickened bark regions) limited *V. mali* colonization and its spread. In particular, MdUGT88F1-RNAi apple stems were characterized by thickened bark and reduced xylem (Dare et al., 2017). Past work has shown that *V. mali* mainly infected host bark and resulted in tissue necrosis but that it could not degrade xylem vessels effectively (Yin et al., 2015). In our investigation, we found that resistant apple trees were characterized primarily by tough bark.

Overall, many pleiotropic changes were induced by *MdUGT88F1* silencing (e.g. increases in SA level and *PR* expression, decreases in lignin and myoinositol content, and changes in cell morphology and tissue). However, it is still unclear how decreased phloridzin biosynthesis resulted directly in these pleiotropic changes in MdUGT88F1-RNAi apple lines. Moreover, these changes enhanced resistance to *Valsa* canker, along with the direct role played by phloridzin as a sugar alternative and a toxin accelerator by *V. mali* through a cocktail effect. However, the extent to which these changes contributed to pathogen susceptibility remains unclear; this needs to be investigated in the future. At any rate, we still believe it is promising to coordinate apple growth vigor and pathogen resistance by regulating the biosynthesis of MdUGT88F1-mediated phloridzin accurately.

CONCLUSION

In conclusion, we propose a putative working model for phloridzin biosynthesis that is necessary for regulating plant development and *Valsa* canker resistance in apple (Fig. 10). In nature, a normal level of phloridzin biosynthesis maintains well-balanced cell wall deposition and supports vigorous growth in apple. However, following infection with *V. mali*, MdUGT88F1-mediated phloridzin biosynthesis is decreased through a currently unknown mechanism. This causes lignin reduction and disorders of cell wall polysaccharides by indirectly modulating flux through the phenylpropanoid pathway and myoinositol metabolism, respectively. Modified cell wall deposition subsequently stimulates the accumulation of SA and ROS. Although modified cell wall deposition results in growth reductions, tissue reinforcements (e.g. in epidermis and bark) ultimately inhibit infection by *V. mali* along with increases in SA and ROS. Meanwhile, decreased phloridzin biosynthesis delays growth and toxin production of *V. mali* and promotes ROS accumulation, ultimately optimizing apple trees for defense against *V. mali*.

MATERIALS AND METHODS

Materials and Growth Conditions

Seeds of Arabidopsis (*Arabidopsis thaliana*) 'Columbia-0' (Col-0) and homozygous T3 transgenic lines were surface-sterilized and plated on MS medium. After stratification at 4°C for 3 d, the plates were exposed to white light (photosynthetically active radiation of 100–150 μE m^{-2} s^{-1}) for 10 d. The light-grown seedlings were transferred to soil and grown at 22°C under a 16-h-light/8-h-dark cycle.

The mature leaves of 'Royal Gala' apple (*Malus domestica*) were used in gene and promoter cloning. GL-3, which is a line with a high regeneration capacity isolated from cv Royal Gala, was used in genetic transformation (Dai et al., 2013). GL-3 tissue-cultured plants were subcultured every 4 weeks. After rooting on MS agar medium, transgenic and nontransgenic apple plantlets were

transferred to small plastic pots (8 × 8 cm) that contained a mixture of soil and perlite (1:1, v/v). After 15 d of acclimation in a growth chamber, the plants were moved to large plastic pots filled with soil and grown in the glasshouse. They were watered regularly and supplied with one-half-strength Hoagland nutrient solution (pH 6) once per week.

One-year-old twigs of the same size from healthy trees of 68 *Malus* spp. accessions were collected from July to August 2017 (Supplemental Table S4) from the Horticultural Experimental Station of Northwest A&F University, Yangling (34°20 N, 108°24 E), China, and were subsequently used in the correlation analysis between DHCs and *Valsa* canker resistance. The *Valsa mali* strain 03-8 was cultured on PDA or PDB in the dark at 25°C (Yin et al., 2015).

Construction of Plasmids and Generation of Transgenic Arabidopsis and Apple Plants

To construct transgenic Arabidopsis plants that expressed the *GUS* gene driven by the *MdUGT88F1* (*ProMdUGT88F1:GUS*/Col-0) or *MdUGT88F4* (*ProMdUGT88F4:GUS*/Col-0) promoter, 2,247- and 2,230-bp genomic promoter sequences upstream of the coding region of *MdUGT88F1* and *MdUGT88F4* were amplified separately and transferred to the binary vector pGWB433. The resultant constructs were transferred into *Agrobacterium tumefaciens* GV3101, and Arabidopsis plants were transformed by the floral dip method (Clough and Bent, 1998).

To generate transgenic apple lines, the coding region of *MdUGT88F1* was cloned and introduced into the vectors pCambia2300 and pGWB411 to create two overexpressing constructs. The vectors pHellsgate2 and pK7WIWG2D were used as RNAi-mediated vectors for silencing *MdUGT88F1*, as described previously by Zhou et al. (2017). Afterward, *A. tumefaciens*-mediated transformation of apple was carried out using GL-3 as the genetic background and strain EHA105 (Dai et al., 2013). The primers used for constructing all vectors are shown in Supplemental Table S5.

RNA Extraction, DNA Isolation, and RT-qPCR Analysis

Total RNA was extracted using a Plant RNA Isolation Kit from Wolact. Genomic DNA was isolated with a Wolact Plant Genomic DNA Purification Kit. RT-qPCR analysis was carried out as previously described by Zhou et al. (2017). Primers used are listed in Supplemental Table S5.

Quantification of DHCs

Quantification of DHCs (including phloretin, phloridzin, trilobatin, and sieboldin) in *Malus* spp. samples was performed as described previously by Zhou et al. (2017).

Morphology Analysis

Shoot height, stem diameter, node number, branch number, leaf length and width, and root dry weight were measured directly after harvesting. Total root length, root surface area, root volume, and average diameter and forks were measured using a Winrhizo 2002 (Regent). At least five biological replicates were performed for each measurement.

Complementation and Depletion Assays

For the complementation assay, the main shoots of GL-3 and transgenic apple plantlets after 4 weeks of subculturing were cut into 1.5-cm segments that included the first two leaves, and then these cuttings were transplanted in subculture MS medium that contained either 0.1% (v/v) ethyl alcohol or 250 μM phloridzin dissolved in ethyl alcohol under long-day conditions (14-h/10-h light/dark cycle) at 23°C. Plants were photographed and growth parameters were recorded after 80 d of subculture. For the depletion assay, the 1.5-cm segments were transplanted either in normal medium or myoinositol-depleted MS regeneration medium. After 35 d of treatment, plants were photographed and growth parameters were measured.

GUS Staining

GUS staining was performed as described by Guo et al. (2017).

Histochemical Analysis

Tissue was excised from stems, leaves, and roots of 38-d-old transgenic apple lines and GL-3 and fixed in an FAA (formalin-aceto-alcohol) solution for 24 h. The fixed tissues were dehydrated using a series of different ethanol concentrations, permeated with wax, and embedded in wax. Sections were sliced at a thickness of 10 μm for Toluidine Blue O and for Mäule and Wiesner staining (Nakashima et al., 2008; Trabucco et al., 2013).

Determination of Lignin and Cell Wall Polysaccharide Concentrations

The stems and roots of transgenic apple lines and GL-3 were dried at 45°C for 14 d and then milled to a fine powder. The lignin content was determined with CWR using the AcBr method (Van Acker et al., 2013). The cellulose content of stems was measured according to Saleme et al. (2017). Extraction and measurement of pectic materials were described by Gallego-Giraldo et al. (2011b).

Assays of Infection, Fungal Growth, and Toxins

The *V. mali* strain 03-8 was cultured on PDA for 3 d. Agar plugs (5 mm each) were taken from the margin of the growing colony of the strain. One-year-old twigs of the same size from healthy apple trees and both stems (2 months old) and expanding leaves (38 d old) of the transgenic apple line and GL-3 were inoculated using stab inoculation (leaves) and the hole puncher wounding method (twigs and stems; Wei et al., 2010). Inoculated leaves and stems were incubated at 25°C for 3 d, and inoculated twigs were incubated at 25°C for 6 d. The lesion sizes of leaves were measured by the crossing method. The total length of longitudinal lesions along twigs and stems was measured directly as the size of the lesions. All leaves and bark (15-cm-long twigs) were collected, immediately frozen in liquid nitrogen, and stored at −80°C before analysis of gene expression, DHC levels, enzymatic activity, phytohormone content, and H_2O_2 level.

To evaluate the effects of phloridzin and phloretin on growth of strain 03-8, agar plugs (5 mm each) from the margin of one growing colony on PDA were incubated on normal and Glc-depleted PDA/PDB with or without phloridzin or phloretin. Growth rates of strain 03-8 were calculated using the expansion of the colony diameters or OD_{600} values. The residual liquid of the incubated PDB was used to determine DHCs quantitatively after strain 03-8 was removed using centrifugation and a 0.22-μm syringe filter. Meanwhile, the toxic effects of the residual liquid from the PDB culture of *V. mali* on leaves of 2-month-old *Malus prunifolia* (obtained from tissue culture) grown in a greenhouse were measured by the simple leaf-puncture assay. A 20-μL aliquot was inoculated in punctured leaves once per day for 5 d.

Assays for Enzymatic Activity

The activity of β-glucosidases (EC 3.2.1.21) of apple bark in response to infection of *V. mali* was measured as described by Gaucher et al. (2013a).

Measurement of Phytohormone Levels

SA and JA were extracted and purified as described by Fu et al. (2012). Briefly, a 50-μL aliquot of extracting solution was air dried with nitrogen gas before being dissolved in 250 μL of sodium acetate (0.1 M, pH 5.5), after which it was treated with 10 μL of β-glucosidase (1 unit μL^{-1}) and hydrolyzed at 37°C for 2 h. After the hydrolysate was denatured in boiling water for 5 min and centrifuged at 13,000*g* for 10 min at 4°C to pellet the protein, the supernatant was used to determine total SA content. A 5-μL aliquot was loaded into the liquid chromatography-mass spectrometry system (Sciex; QTRAP5500) equipped with an InertSustain AQ-C18 column (5-μm particle size, 4.6 mm × 150 mm; GL Sciences) at a flow rate of 0.7 mL min^{-1}. The solvent system consisted of water that contained 0.1% (v/v) formic acid (A) and methanol (B). The gradient followed 75% A (0 min), 75% A (1 min), 5% A (5 min), 5% A (6.5 min), 75% A (6.6 min), and 75% A (13 min).

Evaluation of H_2O_2 and O_2^-

Accumulations of H_2O_2 and O_2^- were examined by histochemical staining methods that used DAB and NBT, respectively (Hu et al., 2018). Quantitative

H_2O_2 measurement was performed using detection kits based on the manufacturer's instructions (Suzhou Comin Biotechnology).

Metabolome Analysis

The fourth and fifth leaves of 38-d-old GL-3 and RNAi apple lines from the top of each plant were collected, frozen immediately in liquid nitrogen, and stored at −80°C. Then, the leaves were delivered to Metware Biotechnology to analyze the widely targeted metabolome (Chen et al., 2013). Soluble sugars and sugar alcohols were verified according to the protocol of Hu et al. (2018).

RNA-Seq

The plant materials used for RNA-seq analysis were the same as the materials used in the metabolome analysis. After filtrating the adapter and low-quality reads, clean reads were aligned to the reference genome GDDH13 of apple (https://iris.angers.inra.fr/gddh13/the-apple-genome-downloads.html) by HISAT2 (Kim et al., 2015). FeatureCounts (Liao et al., 2014) was used to count the reads numbers that were mapped to each gene. DESeq2 was applied for differential gene expression analysis (Love et al., 2014). The resulting *P* values were adjusted by the Benjamini-Hochberg approach to control for a false discovery rate. Genes with $\log_2$ fold change ≥ 1 and false discovery rate < 0.05 were considered to be expressed differentially. The differentially expressed genes were further analyzed with Gene Ontology and Kyoto Encyclopedia of Genes and Genomes (http://www.genome.jp/kegg/) analyses. ClusterProfiler software was adopted for Gene Ontology enrichment analysis (Yu et al., 2012), and the Benjamini and Hochberg approach was also used to test the statistical enrichment of differentially expressed genes in the Kyoto Encyclopedia of Genes and Genomes pathway.

Statistical Analysis

SPSS software (version 17.0) was used for statistical analysis. Data were subjected to one-way ANOVA and reported as means ± SD.

Accession Numbers

Sequence data from this article can be found in the GenBank/EMBL data libraries under the following accession numbers: MdUGT88F1 (KX639791), MdUGT88F4 (KX639792), MdPh-4′-OGT (AY786997), MdPAL (XM_008389362.2), MdCHS (AAY45748), MdCHI (XM_008371941.2), MdPR1 (GU317941), MdPR2 (AY548364.1), MdPR4 (JQ342967.1), MdPR5 (DQ318213.1), MdPR8 (DQ318214.1), MdCOI1 (XM_008383757.2), MdPLD (XM_008375733.2), MdJMT (XM_008389809.2), and VmG6PDH (KC248180).

Supplemental Data

The following supplemental materials are available.

Supplemental Figure S1. Identification of transgenic apple lines.

Supplemental Figure S2. Phenotypes of the 3-month-old GL-3 and Ri-3.

Supplemental Figure S3. Spatial expression of *MdUGT88F1* and *MdUGT88F4*.

Supplemental Figure S4. Cell wall deposition of the stems in the 38-d-old transgenic apple lines and GL-3.

Supplemental Figure S5. Relationship between *Valsa* canker resistance and DHC concentration.

Supplemental Figure S6. Effects of phloridzin and phloretin on *V. mali*.

Supplemental Figure S7. Expression changes in phloridzin biosynthesis-related genes in susceptible ZD1 and resistant ZH16 apple bark in response to *V. mali* infection.

Supplemental Figure S8. Involvement of SA in *Valsa* canker resistance in apple.

Supplemental Figure S9. Involvement of JA in *Valsa* canker resistance in apple.

Supplemental Table S1. Phenotypes of transgenic and nontransgenic apple plants.

Supplemental Table S2. Differentially-expressed genes involved in phloridzin biosynthesis, lignin biosynthesis, myoinositol metabolism, and plant-pathogen interactions, which were revealed in RNAi apple lines compared with GL-3 by RNA-seq analysis.

Supplemental Table S3. Metabolites involved in growth and defense in leaves from RNAi apple lines and GL-3.

Supplemental Table S4. DHC profiles and *Valsa* canker resistance in *Malus* spp.

Supplemental Table S5. Primers used in this study.

ACKNOWLEDGMENTS

We thank Dr. Zhihong Zhang, Shenyang Agricultural University, for providing tissue-cultured GL-3 plants, Lili Huang, Northwest A&F University, for providing *V. mali* strain 03-8, and Thomas A. Gavin, Professor Emeritus, Cornell University, for help with editing the article.

Received April 23, 2019; accepted June 9, 2019; published June 21, 2019.

LITERATURE CITED

Abe K, Kotoda N, Kato H, Soejima J (2007) Resistance sources to *Valsa* canker (*Valsa ceratosperma*) in a germplasm collection of diverse *Malus* species. Plant Breed **126:** 449–453

Apel K, Hirt H (2004) Reactive oxygen species: Metabolism, oxidative stress, and signal transduction. Annu Rev Plant Biol **55:** 373–399

Besseau S, Hoffmann L, Geoffroy P, Lapierre C, Pollet B, Legrand M (2007) Flavonoid accumulation in Arabidopsis repressed in lignin synthesis affects auxin transport and plant growth. Plant Cell **19:** 148–162

Bessho H, Tsuchiya S, Soejima J (1994) Screening methods of apple trees for resistance to *Valsa* canker. Euphytica **77:** 15–18

Bruggeman Q, Prunier F, Mazubert C, de Bont L, Garmier M, Lugan R, Benhamed M, Bergounioux C, Raynaud C, Delarue M (2015) Involvement of Arabidopsis Hexokinase1 in cell death mediated by *myo*-inositol accumulation. Plant Cell **27:** 1801–1814

Chaouch S, Noctor G (2010) *Myo*-inositol abolishes salicylic acid-dependent cell death and pathogen defence responses triggered by peroxisomal hydrogen peroxide. New Phytol **188:** 711–718

Chen W, Gong L, Guo Z, Wang W, Zhang H, Liu X, Yu S, Xiong L, Luo J (2013) A novel integrated method for large-scale detection, identification, and quantification of widely targeted metabolites: Application in the study of rice metabolomics. Mol Plant **6:** 1769–1780

Chen Z, Zheng Z, Huang J, Lai Z, Fan B (2009) Biosynthesis of salicylic acid in plants. Plant Signal Behav **4:** 493–496

Clough SJ, Bent AF (1998) Floral dip: A simplified method for Agrobacterium-mediated transformation of Arabidopsis thaliana. Plant J **16:** 735–743

Cui M, Liang D, Wu S, Ma F, Lei Y (2013) Isolation and developmental expression analysis of L-*myo*-inositol-1-phosphate synthase in four *Actinidia* species. Plant Physiol Biochem **73:** 351–358

Dai H, Li W, Han G, Yang Y, Ma Y, Li H, Zhang Z (2013) Development of a seedling clone with high regeneration capacity and susceptibility to *Agrobacterium* in apple. Sci Hortic (Amsterdam) **164:** 202–208

Dare AP, Hellens RP (2013) RNA interference silencing of CHS greatly alters the growth pattern of apple (Malus × domestica). Plant Signal Behav **8:** e25033

Dare AP, Tomes S, Jones M, McGhie TK, Stevenson DE, Johnson RA, Greenwood DR, Hellens RP (2013) Phenotypic changes associated with RNA interference silencing of chalcone synthase in apple (*Malus* × *domestica*). Plant J **74:** 398–410

Dare AP, Yauk YK, Tomes S, McGhie TK, Rebstock RS, Cooney JM, Atkinson RG (2017) Silencing a phloretin-specific glycosyltransferase perturbs both general phenylpropanoid biosynthesis and plant development. Plant J **91:** 237–250

Daudi A, Cheng Z, O'Brien JA, Mammarella N, Khan S, Ausubel FM, Bolwell GP (2012) The apoplastic oxidative burst peroxidase in

Arabidopsis is a major component of pattern-triggered immunity. Plant Cell **24:** 275–287

Dugé de Bernonville T, Guyot S, Paulin JP, Gaucher M, Loufrani L, Henrion D, Derbré S, Guilet D, Richomme P, Dat JF, et al (2010) Dihydrochalcones: Implication in resistance to oxidative stress and bioactivities against advanced glycation end-products and vasoconstriction. Phytochemistry **71:** 443–452

Feng H, Xu M, Zheng X, Zhu T, Gao X, Huang L (2017) MicroRNAs and their targets in apple (*Malus domestica* cv. "Fuji") involved in response to infection of pathogen *Valsa mali*. Front Plant Sci **8:** 2081

Fu J, Chu J, Sun X, Wang J, Yan C (2012) Simple, rapid, and simultaneous assay of multiple carboxyl containing phytohormones in wounded tomatoes by UPLC-MS/MS using single SPE purification and isotope dilution. Anal Sci **28:** 1081–1087

Gallego-Giraldo L, Escamilla-Trevino L, Jackson LA, Dixon RA (2011a) Salicylic acid mediates the reduced growth of lignin down-regulated plants. Proc Natl Acad Sci USA **108:** 20814–20819

Gallego-Giraldo L, Jikumaru Y, Kamiya Y, Tang Y, Dixon RA (2011b) Selective lignin downregulation leads to constitutive defense response expression in alfalfa (*Medicago sativa* L.). New Phytol **190:** 627–639

Gaucher M, Dugé de Bernonville T, Guyot S, Dat JF, Brisset MN (2013a) Same ammo, different weapons: Enzymatic extracts from two apple genotypes with contrasted susceptibilities to fire blight (Erwinia amylovora) differentially convert phloridzin and phloretin in vitro. Plant Physiol Biochem **72:** 178–189

Gaucher M, Dugé de Bernonville T, Lohou D, Guyot S, Guillemette T, Brisset MN, Dat JF (2013b) Histolocalization and physico-chemical characterization of dihydrochalcones: Insight into the role of apple major flavonoids. Phytochemistry **90:** 78–89

Gilchrist DG (1998) Programmed cell death in plant disease: The purpose and promise of cellular suicide. Annu Rev Phytopathol **36:** 393–414

Glazebrook J (2005) Contrasting mechanisms of defense against biotrophic and necrotrophic pathogens. Annu Rev Phytopathol **43:** 205–227

Gosch C, Halbwirth H, Kuhn J, Miosic S, Stich K (2009) Biosynthesis of phloridzin in apple (*Malus domestica* Borkh.). Plant Sci **176:** 223–231

Gosch C, Halbwirth H, Schneider B, Hölscher D, Stich K (2010) Cloning and heterologous expression of glycosyltransferases from *Malus* × *domestica* and *Pyrus communis*, which convert phloretin to phloretin 2′-*O*-glucoside (phloridzin). Plant Sci **178:** 299–306

Guo P, Li Z, Huang P, Li B, Fang S, Chu J, Guo H (2017) A tripartite amplification loop involving the transcription factor WRKY75, salicylic acid, and reactive oxygen species accelerates leaf senescence. Plant Cell **29:** 2854–2870

Gutierrez BL, Zhong G, Brown SK (2018) Genetic diversity of dihydrochalcone content in *Malus* germplasm. Genet Resour Crop Evol **65:** 1485–1502

Hu L, Zhou K, Li Y, Chen X, Liu B, Li C, Gong X, Ma F (2018) Exogenous *myo*-inositol alleviates salinity-induced stress in *Malus hupehensis* Rehd. Plant Physiol Biochem **133:** 116–126

Huot B, Yao J, Montgomery BL, He SY (2014) Growth-defense tradeoffs in plants: A balancing act to optimize fitness. Mol Plant **7:** 1267–1287

Hutabarat OS, Flachowsky H, Regos I, Miosic S, Kaufmann C, Faramarzi S, Alam MZ, Gosch C, Peil A, Richter K, et al (2016) Transgenic apple plants overexpressing the *chalcone 3-hydroxylase* gene of *Cosmos sulphureus* show increased levels of 3-hydroxyphloridzin and reduced susceptibility to apple scab and fire blight. Planta **243:** 1213–1224

Ke X, Huang L, Han Q, Gao X, Kang Z (2013) Histological and cytological investigations of the infection and colonization of apple bark by *Valsa mali var. mali*. Australas Plant Pathol **42:** 85–93

Kim D, Langmead B, Salzberg SL (2015) HISAT: A fast spliced aligner with low memory requirements. Nat Methods **12:** 357–360

Koganezawa H, Sakuma T (1982) Possible role of breakdown products of phloridzin in symptom development by *Valsa ceratosperma*. Ann Phytopathol Soc Jpn **48:** 521–528

Lee Y, Chen F, Gallego-Giraldo L, Dixon RA, Voit EO (2011) Integrative analysis of transgenic alfalfa (*Medicago sativa* L.) suggests new metabolic control mechanisms for monolignol biosynthesis. PLOS Comput Biol **7:** e1002047

León J, Shulaev V, Yalpani N, Lawton MA, Raskin I (1995) Benzoic acid 2-hydroxylase, a soluble oxygenase from tobacco, catalyzes salicylic acid biosynthesis. Proc Natl Acad Sci USA **92:** 10413–10417

Li X, Bonawitz ND, Weng JK, Chapple C (2010) The growth reduction associated with repressed lignin biosynthesis in *Arabidopsis thaliana* is independent of flavonoids. Plant Cell **22:** 1620–1632

Liao Y, Smyth GK, Shi W (2014) featureCounts: An efficient general purpose program for assigning sequence reads to genomic features. Bioinformatics **30:** 923–930

Love MI, Huber W, Anders S (2014) Moderated estimation of fold change and dispersion for RNA-seq data with DESeq2. Genome Biol **15:** 550

Meng D, Li C, Park HJ, González J, Wang J, Dandekar AM, Turgeon BG, Cheng L (2018) Sorbitol modulates resistance to *Alternaria alternata* by regulating the expression of an *NLR* resistance gene in apple. Plant Cell **30:** 1562–1581

Nakashima J, Chen F, Jackson L, Shadle G, Dixon RA (2008) Multi-site genetic modification of monolignol biosynthesis in alfalfa (*Medicago sativa*): Effects on lignin composition in specific cell types. New Phytol **179:** 738–750

Natsume H, Seto H, Haruo S, Ôtake N (1982) Studies on apple canker disease: The necrotic toxins produced by *Valsa ceratosperma*. Agric Biol Chem **46:** 2101–2106

Oliver RP, Friesen TL, Faris JD, Solomon PS (2012) Stagonospora nodorum: From pathology to genomics and host resistance. Annu Rev Phytopathol **50:** 23–43

Saleme MLS, Cesarino I, Vargas L, Kim H, Vanholme R, Goeminne G, Van Acker R, Fonseca FCA, Pallidis A, Voorend W, et al (2017) Silencing CAFFEOYL SHIKIMATE ESTERASE affects lignification and improves saccharification in poplar. Plant Physiol **175:** 1040–1057

Shirley BW, Kubasek WL, Storz G, Bruggemann E, Koornneef M, Ausubel FM, Goodman HM (1995) Analysis of *Arabidopsis* mutants deficient in flavonoid biosynthesis. Plant J **8:** 659–671

Sun Q, Liu X, Yang J, Liu W, Du Q, Wang H, Fu C, Li WX (2018) MicroRNA528 affects lodging resistance of maize by regulating lignin biosynthesis under nitrogen-luxury conditions. Mol Plant **11:** 806–814

Suzuki N, Miller G, Morales J, Shulaev V, Torres MA, Mittler R (2011) Respiratory burst oxidases: The engines of ROS signaling. Curr Opin Plant Biol **14:** 691–699

Tanaka S, Han X, Kahmann R (2015) Microbial effectors target multiple steps in the salicylic acid production and signaling pathway. Front Plant Sci **6:** 349

Trabucco GM, Matos DA, Lee SJ, Saathoff AJ, Priest HD, Mockler TC, Sarath G, Hazen SP (2013) Functional characterization of cinnamyl alcohol dehydrogenase and caffeic acid *O*-methyltransferase in *Brachypodium distachyon*. BMC Biotechnol **13:** 61

Valluru R, Van den Ende W (2011) *Myo*-inositol and beyond: Emerging networks under stress. Plant Sci **181:** 387–400

Van Acker R, Vanholme R, Storme V, Mortimer JC, Dupree P, Boerjan W (2013) Lignin biosynthesis perturbations affect secondary cell wall composition and saccharification yield in *Arabidopsis thaliana*. Biotechnol Biofuels **6:** 46

Vanholme R, Morreel K, Ralph J, Boerjan W (2008) Lignin engineering. Curr Opin Plant Biol **11:** 278–285

Vlot AC, Dempsey DA, Klessig DF (2009) Salicylic acid, a multifaceted hormone to combat disease. Annu Rev Phytopathol **47:** 177–206

Wang C, Li C, Li B, Li G, Dong X, Wang G, Zhang Q (2014) Toxins produced by *Valsa mali* var. *mali* and their relationship with pathogenicity. Toxins (Basel) **6:** 1139–1154

Wang P, Yin L, Liang D, Li C, Ma F, Yue Z (2012) Delayed senescence of apple leaves by exogenous melatonin treatment: Toward regulating the ascorbate-glutathione cycle. J Pineal Res **53:** 11–20

Wei J, Huang L, Gao Z, Ke X, Kang Z (2010) Laboratory evaluation methods of apple *Valsa* canker disease caused by *Valsa ceratosperma* sensu Kobayashi. Acta Phytopathologica Sin **40:** 14–20

Wildermuth MC, Dewdney J, Wu G, Ausubel FM (2001) Isochorismate synthase is required to synthesize salicylic acid for plant defence. Nature **414:** 562–565

Xiao Z, Zhang Y, Chen X, Wang Y, Chen W, Xu Q, Li P, Ma F (2017) Extraction, identification, and antioxidant and anticancer tests of seven dihydrochalcones from *Malus* 'Red Splendor' fruit. Food Chem **231:** 324–331

Yahyaa M, Davidovich-Rikanati R, Eyal Y, Sheachter A, Marzouk S, Lewinsohn E, Ibdah M (2016) Identification and characterization of UDP-glucose:phloretin 4′-O-glycosyltransferase from Malus × domestica Borkh. Phytochemistry **130:** 47–55

Ye W, Ren W, Kong L, Zhang W, Wang T (2016) Transcriptomic profiling analysis of *Arabidopsis thaliana* treated with exogenous *myo*-inositol. PLoS ONE **11:** e0161949

Yin Z, Liu H, Li Z, Ke X, Dou D, Gao X, Song N, Dai Q, Wu Y, Xu JR, et al (2015) Genome sequence of *Valsa* canker pathogens uncovers a potential adaptation of colonization of woody bark. New Phytol **208:** 1202–1216

Yin Z, Ke X, Kang Z, Huang L (2016a) Apple resistance responses against *Valsa mali* revealed by transcriptomics analyses. Physiol Mol Plant Pathol **93:** 85–92

Yin Z, Zhu B, Feng H, Huang L (2016b) Horizontal gene transfer drives adaptive colonization of apple trees by the fungal pathogen *Valsa mali*. Sci Rep **6:** 33129

Yu G, Wang LG, Han Y, He QY (2012) clusterProfiler: An R package for comparing biological themes among gene clusters. OMICS **16:** 284–287

Zhang M, Feng H, Zhao Y, Song L, Gao C, Xu X, Huang L (2018) *Valsa mali* pathogenic effector VmPxE1 contributes to full virulence and interacts with the host peroxidase MdAPX1 as a potential target. Front Microbiol **9:** 821

Zhang XZ, Zhao YB, Li CM, Chen DM, Wang GP, Chang RF, Shu HR (2007) Potential polyphenol markers of phase change in apple (*Malus domestica*). J Plant Physiol **164:** 574–580

Zhou K, Hu L, Li P, Gong X, Ma F (2017) Genome-wide identification of glycosyltransferases converting phloretin to phloridzin in *Malus* species. Plant Sci **265:** 131–145

Zhou K, Hu L, Liu B, Li Y, Gong X, Ma F (2018) Identification of apple fruits rich in health-promoting dihydrochalcones by comparative assessment of cultivated and wild accessions. Sci Hortic (Amsterdam) **233:** 38–46